



# Propagation of high energy lasers through clouds: modeling and simulation

ANDREW LAWRENCE\*  AND BENJAMIN F. AKERS

Department of Mathematics and Statistics, Air Force Institute of Technology, Dayton, Ohio 45433, USA

\*Corresponding author: [andrew.lawrence.13@us.af.mil](mailto:andrew.lawrence.13@us.af.mil)

Received 17 August 2020; revised 29 September 2020; accepted 12 October 2020; posted 13 October 2020 (Doc. ID 404526); published 11 November 2020

**A model for 10.6  $\mu\text{m}$  high energy laser beam interaction with a uniform, monodisperse cloud of water droplets is developed. The model includes droplet and vapor heating as well as droplet shattering in the “fast regime” as defined in Appl. Opt. 28, 3671 (1989). The cloud dynamics feed back on the laser via changes in the complex refractive index. In one space dimension, the model is solved exactly, including an explicit formula for the front of the cleared channel. Numerical simulations are conducted for the axisymmetric three-dimensional case. Model predictions and limitations are discussed.** © 2020 Optical Society of America

<https://doi.org/10.1364/AO.404526>

## 1. INTRODUCTION

Laser–atmosphere interactions are important in a host of applications including targeting, wireless communication, energy transfer, remote sensing, the measurement of gravity waves, and many more [1–4]. As a result, the propagation of lasers through the atmosphere has been modeled extensively [5–9]. In the optical regime, clouds form an obstacle to laser propagation, lowering the effectiveness of these applications [10–12].

When a high energy laser propagates through a cloud, the possibility exists for the beam to alter the physical properties of the drops (temperature, diameter, shape, etc). The interaction of high energy radiation and water droplets has been studied experimentally [13–18], as well as via modeling and simulation [5–9,19–23]. The physics of laser droplet interaction is complex and depends on droplet geometry, wavelength, potential impurities, and relative droplet size. The primary response of the incoming field may be to scatter off the droplet, to heat the surface, or to heat the interior [24]. In this work, we consider monodisperse, uniform fields of water droplets with diameter of 10  $\mu\text{m}$ , an average drop size in a typical cloud [25], and a 10.6  $\mu\text{m}$  laser. This beam and drop combination results in an order of one Mie size parameter, where the primary effect of droplets on the beam will be volumetric absorption, with corresponding droplet heating.

In this heating regime, inhomogeneities form in the heating source function and lead to the development of hot spots within the droplet [26–28]. Irradiated, pure water droplets do not change phase at 100°C, instead droplets spontaneously nucleate at a critical temperature of  $T_c \approx 305^\circ\text{C}$  [29,30]. We model droplets that are exposed to intense background radiation, with responses falling in the “fast” regime, as described in [19]. In this

regime, heating ultimately results in explosive destruction of droplets [15,31–33]. In the “slow” regime, evaporation balances heating [34–37]. We consider 10  $\mu\text{m}$  droplets, in which regime fluid viscosity dominates convective motion within the drop; for larger millimeter (mm) size droplets, this convection may play an important role [24,38]. We approximate an exploded droplet as being replaced by heated water vapor (dynamics related to smaller pieces of shattered droplets, which may be created via a destruction event are neglected).

In addition to depositing energy in water droplets, the laser will also lose energy into the propagation medium. For near to stagnant backgrounds, this heating feeds back on the beam propagation, leading to thermal blooming [39–42]. Thermal blooming has a long history of study, in circumstances where the fluid propagation medium is prescribed (either fixed or described statistically) [43–47]. Recently, as laser power continues to increase, efforts have been made to couple the fluid flows induced by the laser heating (for example buoyancy driven convection) on the beam’s thermal blooming [48]. This work is essentially a first step toward including suspended particles in the model of [48]. It also extends the model for static lasers in [15] by including beam dynamics, to evaluate long distance propagation potential (both distance and timing), and complements [5] by considering the high power regime. The shattering of monodisperse droplets was studied in [49], where droplet heating and shattering was simulated with a prescribed laser field. The dynamics of both the laser and a monodisperse uniform field of small drops (as model for fog) were modeled in the slow regime (low power) in [50]; we adopt a similar cloud model, but operate in the fast regime (high power), where droplets explode rather than evaporate. Although there is a

long history of modeling and simulation of laser and droplet interactions, this is the first work, to the best of our knowledge, to model and simulate both the droplet and laser dynamics in the high power regime. We also include thermal blooming of the background vapor.

In this work, we study the problem of pulsed, high irradiance laser propagation through a simple cloud model. This model includes droplet heating (during the pulse), cooling (between pulses), and explosive vaporization. The beam propagation is modeled by the paraxial equation, [39,51,52], in which the refractive index is coupled to both background gas temperature and droplet concentration. The model assumes a cloud to be composed of an initially uniform distribution of water droplets suspended in background gas approximated as only containing water vapor. We consider lasers of sufficiently high irradiance ( $|A|_{\text{crit}} \approx 10^4 \frac{\text{W}}{\text{cm}^2}$ ) such that heating happens on a time scale (1.41  $\mu\text{s}$  [53]), for which droplet explosion is the dominant fluid response; our model neglects evaporation and convective fluid motions. We also restrict the power window from above, to avoid plasma formation and self-focusing; these regimes are of separate interest and have their own history of study [19,54–59]. These combined effects of suspended water droplets and background vapor on blooming and dissipation are included. For the wavelength in question, water vapor is more absorbing than dry air, thus it will lead to increased blooming (and decreased clearing). We approximate the background gas as all water vapor (resulting in the most conservative possible clearing estimates). The effects of scattering are acknowledged as important, but neglected for this analysis, as they are small for the wavelength and droplet size choices. In the context of this model, we observe the potential for laser-induced cloud clearing.

The paper is organized as follows. Section 2 presents the problem formulation and modeling assumptions. An exact one-dimensional solution, including an explicit formula for the depth of the cleared channel, is derived in Section 3. The numerical method and results follow in Section 4. A discussion of predictions, limitations, and usefulness of the presented model are in Section 5. We conclude and present opportunities for future research in Section 6.

## 2. FORMULATION

In this section, we present a model for high energy laser propagation through a cloud. The cloud is approximated as a uniform distribution of water droplets suspended in a background gas. The model takes the form of a system of coupled differential equations for the droplet temperature, background gas temperature, and beam intensity.

The beam dynamics are modeled using the paraxial approximation to Maxwell's equations:

$$A_z = \left( \frac{-1}{2ik(\eta_0 + i\beta_0)} \left( \frac{\partial^2}{\partial r^2} + \frac{1}{r} \frac{\partial}{\partial r} \right) + ik(\eta_1 + i\beta_1) \right) A. \quad (1)$$

In the paraxial equation, Eq. (1), the variable  $A$  is the envelope of the electric field. The radial coordinate  $r$  accounts for the transverse direction, while  $z$  represents the propagation direction. The variables  $\eta_0$  and  $\beta_0$  are, respectfully, the

leading-order approximations to real and imaginary parts of the index of refraction. In the derivation of the paraxial equation, a separation of scales is assumed between the longitudinal and transverse directions; the refractive index is also assumed to have fluctuations that are asymptotically small when measured relative to this aspect ratio. The parameters  $\eta_1$  and  $\beta_1$  are the first corrections to the mean refractive index, which correspond to small fluctuations due to changes in the medium's physical state (e.g., temperature changes). The index of refraction of the mixed media, a combination of water droplets and background vapor, is represented by

$$n = Pn_w + (1 - P)n_v, \quad (2)$$

as in [60] according to the rule of mixtures. In Eq. (2), the subscript  $w$  corresponds to the index of refraction of liquid water; the subscript  $v$  corresponds to the index of refraction of the approximated background gas, pure water vapor. The real and imaginary terms, the leading-order terms, and the first-order fluctuations of the index of refraction are all taken to satisfy the rule of mixtures in equations, analogous to Eq. (2). The numerical values for these constants can be found in Table 1. The mixing ratio  $P$  is defined as

$$P = 10^{-6} \frac{D}{D_0}, \quad (3)$$

where  $10^{-6}$  is the droplet concentration in the cloud (the ratio of the volume of the droplets to the volume of the vapor) and equivalent to 2000 droplets per  $\text{cm}^3$  as in [25],  $D_0$  is the initial droplet diameter (10  $\mu\text{m}$ ), and the diameter of the drop,  $D$ , as a function of space and time is defined by

$$D(r, z, t) = \begin{cases} 10 \mu\text{m} & T(\xi) < T_c \\ 0 & T(\xi) \geq T_c \end{cases}, \quad (4)$$

where  $T_c$  is the critical temperature at which droplets spontaneously nucleate and subsequently explode. Equation (4) is the simplest possible model for droplet dynamics that still accounts for droplet shattering. The droplet diameter is assumed to be either constant or absent, as droplet explosion is essentially a threshold process [61]. This approximation makes sense only for fast time scales with high power lasers, in which slower dynamics, e.g., evaporation, are neglected [19,62].

The temperature in individual water droplets is tracked and used to determine time and location explosive vaporization events. The presence, or absence, of droplets feeds back on the laser via the complex refractive index as above. The beam diameter is assumed to be large relative to the droplets, such that the droplets feel a uniform intensity field, which is incident from a uniform spatial direction. We do not solve for the beam intensity within the droplet, but instead assume an interior heating profile based on those reported in [19]. The resulting temperature equation is

$$c\rho T_t = \nabla \cdot (K\nabla T) + \frac{4\pi\eta_{0,w}\beta_{0,w}}{\lambda_0} S(\xi)I, \quad (5)$$

with

$$S(\xi) = \sqrt{\frac{3}{2\pi}} \exp\left(\frac{-9}{2}(\xi - 0.9)^2\right) + 0.8.$$

**Table 1. Numerical Values of Physical Parameters Used for Simulations with References<sup>a</sup>**

Parameter	Description	Value	Units	Source
$\lambda_0$	Wavelength	$10.6 \times 10^{-6}$	m	Model choice
$k$	Wavenumber	$2\pi/\lambda_0 = 5.9 \times 10^5$	$\text{m}^{-1}$	Model choice
$\rho$	Density of Water	$10^3$	$\frac{\text{kg}}{\text{m}^3}$	[19]
$c$	Specific Heat of Water	$4.1855 \times 10^3$	$\frac{\text{J}}{\text{kg}\cdot^\circ\text{C}}$	[19]
$K$	Thermal Conductivity of Water	$5.187 \times 10^{-2}$	$\frac{\text{J}}{\text{s}\cdot\text{m}\cdot^\circ\text{C}}$	[19]
$c_v$	Specific Heat of Vapor	$1.996 \times 10^3$	$\frac{\text{J}}{\text{kg}\cdot^\circ\text{C}}$	[19]
$K_v$	Thermal Conductivity of Vapor	$2.0935 \times 10^{-2}$	$\frac{\text{J}}{\text{s}\cdot\text{m}\cdot^\circ\text{C}}$	[19]
$\eta_{0,w}$	$\text{Re}(n_{\text{water}})$	1.179	-	[19]
$\eta_{1,w}$	$\text{Re}(n_{\text{water}})$ , Fluctuation	0.776405	-	[19]
$\eta_{0,v}$	$\text{Re}(n_{\text{vapor}})$	1	-	[25,65]
$\eta_{1,v}$	$\text{Re}(n_{\text{vapor}})$ , Fluctuation	$3.648 \times 10^{-6} \frac{T_v}{273}$	-	[25,65]
$\beta_{0,w}$	$\text{Im}(n_{\text{water}})$	0.07558	-	[19]
$\beta_{1,w}$	$\text{Im}(n_{\text{water}})$ , Fluctuation	0.03	-	[19]
$\beta_{0,v}$	$\text{Im}(n_{\text{vapor}})$	$3.2 \times 10^{-10}$	-	[63]
$\beta_{1,v}$	$\text{Im}(n_{\text{vapor}})$ , Fluctuation	$8.667 \times 10^{-18} e^{\frac{2838}{T_v}}$	-	[66]

<sup>a</sup>Units are given if the parameter is dimensional.

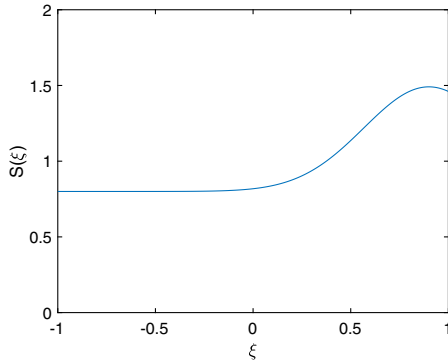


**Fig. 1.** Source function distribution  $S(\xi)$  representing the relative heating of a  $5 \mu\text{m}$  droplet as a function of a normalized internal spatial coordinate,  $\xi$ .

Here,  $c$  is the specific heat of water,  $\rho$  is the density of water,  $K$  is the thermal conductivity of water,  $I$  is the irradiance, and  $S(\xi)$  is a normalized source function representing how much a  $10 \mu\text{m}$  diameter droplet is heated due to radiation as a function of one, normalized, internal space dimension,  $\xi$ , such that  $\xi = 0$  corresponds to the center of the drop,  $\xi = -1$  represents the edge of the drop closest to the laser source, and  $\xi = +1$  is mapped to the edge of the drop furthest from the laser source. The profile of  $S$  can be seen in Fig. 1. A rigorous extension of the heating profile to two and three dimensions would require calculations of the laser refraction through such a droplet. We consider only one-dimensional internal heat profiles; a heuristic extension to higher dimensions would include a corresponding multi-dimensional Gaussian profile, centered near the back of the droplet, along the azimuthal axis.

In Eq. (5) above, the first term on the right side of the equation accounts for thermal diffusion, while the second term represents heat effects due to radiation. Following [19], by setting a ratio of the two terms equal to one and solving for the irradiance, we can determine the irradiance for which the heating term and thermal diffusion term are proportional:

$$I = \frac{\lambda_0 K \nabla^2 T}{4\pi \eta_{0,w} \beta_{0,w} S(\xi)}$$

Given  $\eta_{0,w} = O(1)$ ,  $\beta_{0,w} = O(10^{-1})$ ,  $S = O(1)$ ,  $\lambda_0 = O(10^{-5}) \text{ m}$ ,  $K = O(10^{-1}) \frac{\text{W}}{\text{m}\cdot^\circ\text{C}}$ , and  $\nabla^2 T \approx \frac{\delta T}{(\delta R)^2}$  such that  $\delta T = O(10^2)^\circ\text{C}$  and  $(\delta R)^2 = O(10^{-8}) \text{ cm}^2$ , a critical irradiance of  $I_{\text{crit}} \approx 10^4 \frac{\text{W}}{\text{cm}^2}$  makes the heating term proportional to the thermal diffusion.

For this analysis, we consider a laser with peak irradiance of  $I = 10^6 \frac{\text{W}}{\text{cm}^2} = 1 \frac{\text{MW}}{\text{cm}^2}$ , which allows the heating term to dominate the thermal diffusion while staying below the plasma formation limit of  $10^8 \frac{\text{W}}{\text{cm}^2}$ . We thus neglect diffusion of heat within drops while the beam is on.

The above argument yields a piecewise temperature equation; the heating term dominates when the pulse is on and is nonexistent when the pulse is off. The one-dimensional equation for the droplet temperature, in the normalized internal coordinate  $\xi = z/R$ , is

$$c \rho T_t = \begin{cases} |A| f & \text{(Pulse on)} \\ K T_{\xi\xi} & \text{(Pulse off)} \end{cases} \quad (6)$$

When the pulse is off, the boundary conditions for the heat equation take the form [19]

$$-K \left. \frac{\partial T}{\partial \xi} \right|_{\xi=\Xi^-} = -K_v \left. \frac{\partial T}{\partial \xi} \right|_{\xi=\Xi^+} + mL + mc(T - T_0) + \frac{m^3}{2\rho_v^2}, \quad (7)$$

where  $K_v$  is the thermal conductivity of vapor,  $\rho_v$  is the density of vapor adjacent to the droplet given in Eq. (10), and  $m$  is the mass flux through the surface of the droplet such that  $m > 0$  indicates mass leaving the droplet, and  $m < 0$  is mass entering the droplet. Quantities evaluated at location  $\Xi_{\pm}$  are limits taken from the inside and outside, respectively. The term on the left-hand side of Eq. (7) is the heat flux from inside the drop. On the right-hand side of Eq. (7), the first term is the heat flux from the ambient water vapor outside of the drop, the second

term is the energy used in vaporization on the surface, the third term is the energy loss due to droplet shrinking, and the last term is the convection term, which represents the kinetic energy exchange [19].

We have chosen to operate in the “fast” regime of Armstrong, neglecting evaporation, so the mass flux across each droplet surface,  $m$ , is zero. The only terms left in the boundary condition equation, therefore, relate the thermal diffusivities of each medium, e.g., Eq. (7) becomes

$$-K \left. \frac{\partial T}{\partial \xi} \right|_{\xi=\Xi^-} = -K_v \left. \frac{\partial T}{\partial \xi} \right|_{\xi=\Xi^+}. \quad (8)$$

Just as the droplets are coupled to the laser, so is the background vapor. The large power density and short time-scale assumptions applied to the droplets have similar consequences when applied to the vapor. The droplet and vapor equations are explicitly coupled by their shared boundary equation, Eq. (8). The droplet and vapor equations are also implicitly coupled, as both vapor and droplets affect the beam. In the vapor, however, the absorption is much smaller than the absorption of water,  $\beta_{0,v} \ll \beta_{0,w}$ . Therefore, for the chosen irradiance, the diffusion term must be kept while the pulse is on in the vapor heating equation. The background vapor solves the following equations:

$$c_v \rho_v \frac{\partial T_v}{\partial t} = \begin{cases} f_v |A| + K_v \Delta T_v & \text{(Pulse on)} \\ K_v \Delta T_v & \text{(Pulse off)} \end{cases}, \quad (9)$$

in which the density is taken to satisfy

$$\rho_v = 0.0022 \frac{1}{T_v^{9.2}} \exp\left(77.3450 + 0.0057 T_v - \frac{7235}{T_v}\right), \quad (10)$$

where  $c_v$ ,  $\rho_v$ ,  $K_v$ ,  $f_v$  are the specific heat, density [25], thermal conductivity, and heat production distribution of vapor, respectively. It should be noted that there is no corresponding normalized source function,  $S_v(\xi)$ , for vapor heating; there are no geometric effects in the vapor absorption. The vapor also affects the beam through the index of refraction. The corrections to both the real and the imaginary part,  $\eta_{1,v}$  and  $\beta_{1,v}$ , depend on the temperature of the vapor:

$$|A|(z) = \begin{cases} |A|(0) \exp(-k\beta_{1,w}z) & t < t_c(0) \\ |A|(0) \exp(-k\beta_{1,v}z) & z < z_c(t) \\ |A|(0) \exp(-k\beta_{1,v}z_c(t)) \exp(-k\beta_{1,w}(z - z_c(t))) & z > z_c(t) \end{cases}, \quad (11)$$

$$\eta_{1,v} = 3.648 \times 10^{-6} \frac{T_v}{273} \quad \text{and}$$

$$\beta_{1,v} = 8.667 \times 10^{-18} \exp\left(\frac{2838}{T_v}\right).$$

For the numerical simulations in Section 4, we have used the full dependence of the vapor on temperature. In our numerical simulation, we observe a negligible contribution from the temperature dependence of the absorptivity,  $\beta_{1,v}$ . In Section 3, we

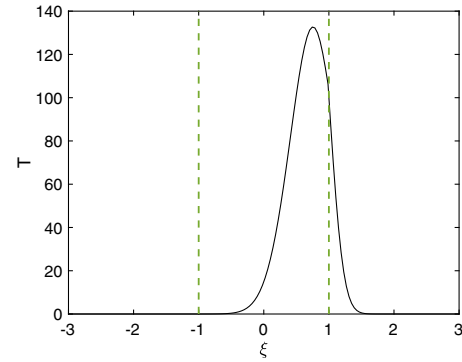


**Fig. 2.** Temperature of an arbitrary droplet and its surrounding vapor in one dimension after one heating and cooling period using  $10^6 \frac{\text{W}}{\text{cm}^2}$  irradiance laser. The droplet boundary is labeled by vertical lines, and the scale is in units of droplet diameter.

approximate  $\beta_{1,v} \approx 3 \times 10^{-13}$ , allowing for the construction of an exact solution for the front of the cleared region as it passes through the cloud. This approximate  $\beta_{1,v}$  appears in [63].

In the above model, both the vapor and the drops are heated. We directly simulate the coupled system of Eqs. (6) and (9) in a small vapor domain local to a drop. In this domain, we observe local heat transfer from droplets to the surrounding vapor. The effect of the surface heat transfer is visualized in Fig. 2 after one heating and one cooling period. The global vapor temperature is updated at the same time as the droplet temperature by a rule of mixtures-based coupling.

### 3. SHATTERING FRONT: EXACT SOLUTION

For a one-dimensional beam, e.g., neglecting diffraction by setting  $\partial_r A \equiv 0$  in Eq. (1), the equations for the beam and droplet temperature fields are a pair of coupled linear differential equations, which are exactly solvable in terms of exponentials. The only non-trivial detail of the solution procedure is that we allow for a shattering front to propagate through the system, creating a discontinuous distribution of droplet radii. We are able to explicitly determine the location in space–time of the front of the cleared region while the pulse is constantly on. The details of this solution follow.

The exact solution to Eq. (1) with  $\partial_r A = 0$  is

where  $t_c(z)$  is the time at which the droplets at location  $z$  shatter, and  $z_c(t)$  is the location of the cleared front as a function of time. It should be noted that by setting  $\partial_r A = 0$ , the  $\beta_0$  and  $\eta_0$  terms are eliminated, and the  $\eta_1$  terms cancel out when solving Eq. (1).

Equation (11) does not include a prescription for  $t_c$  or  $z_c$  and thus is an incomplete representation of the solution. However, we can find an explicit solution by first solving for the temperature along the cleared front.

The temperature at the droplet interface is

$$\begin{aligned}
 T(z, t_c(z)) &= \int_0^{t_c(z)} C|A|(z, t) dt \\
 &= t_c(0)C|A|(0) \exp(-k\beta_{1,w}z) \\
 &\quad + \exp(-k\beta_{1,w}z) \int_{t_c(0)}^{t_c(z)} C|A|(0) \\
 &\quad \times \exp(-k(\beta_{1,v} - \beta_{1,w})z_c(t)) dt, \quad (12)
 \end{aligned}$$

where  $C = \max_{\xi \in [-1,1]} f(\xi) = \frac{2\sqrt{2\pi}}{\lambda_0} \eta_{1,w} \beta_{1,w}$ .

It should be noted that the temperature along the front,  $T(z, t_c(z))$ , is by definition fixed; it is the critical temperature at which droplets explode,  $T_c$  in Eq. (4). To solve for  $t_c$ , we differentiate Eq. (12) with respect to  $z$  yielding

$$\begin{aligned}
 \frac{dT}{dz} = 0 &= -t_c(0)k\beta_{1,w}C|A|(0) \exp(-k\beta_{1,w}z) \\
 &\quad + C|A|(0) \exp(-k(\beta_{1,v} - \beta_{1,w})z_c(t_c(z))) \\
 &\quad \times \exp(-k\beta_{1,w}z) t'_c(z) \\
 &\quad - k\beta_{1,w} \exp(-k\beta_{1,w}z) \int_{t_c(0)}^{t_c(z)} C|A|(0) \\
 &\quad \times \exp(-k(\beta_{1,v} - \beta_{1,w})z_c(t)) dt. \quad (13)
 \end{aligned}$$

The substitution  $u = z_c(t)$  paired with the fact that  $z_c$  and  $t_c$  are inverse functions of one allows Eq. (15) to be rewritten as

$$\begin{aligned}
 0 &= -t_c(0)k\beta_{1,w} + \exp(-k(\beta_{1,v} - \beta_{1,w})z) t'_c(z) \\
 &\quad - k\beta_{1,w} \int_0^z \exp(-k(\beta_{1,v} - \beta_{1,w})u) \frac{du}{z'_c(t_c(u))}. \quad (14)
 \end{aligned}$$

Further use of the inverse relationship of  $z_c$  and  $t_c$ ,

$$u = z_c(t_c(u)), \quad \text{and thus} \quad 1 = z'_c(t_c(u))t'_c(u),$$

allows Eq. (14) to be written as

$$\begin{aligned}
 0 &= -t_c(0)k\beta_{1,w} + \exp(-k(\beta_{1,v} - \beta_{1,w})z) t'_c(z) \\
 &\quad - k\beta_{1,w} \int_0^z \exp(-k(\beta_{1,v} - \beta_{1,w})u) t'_c(u) du. \quad (15)
 \end{aligned}$$

Differentiating Eq. (15) with respect to  $z$  and simplifying returns a linear constant-coefficient differential equation:

$$k\beta_{1,v}t'_c(z) = t''_c(z). \quad (16)$$

The solution to Eq. (16) is

$$t_c(z) = \frac{T_c}{|A(0,0)|C} \left( \frac{\beta_{1,w}}{\beta_{1,v}} (e^{k\beta_{1,v}z} - 1) + 1 \right), \quad (17)$$

which can be inverted to produce

$$z_c(t) = \frac{1}{k\beta_{1,v}} \ln \left[ \frac{\beta_{1,v}}{\beta_{1,w}} \left( \frac{t|A(0,0)|C}{T_c} - 1 \right) + 1 \right]. \quad (18)$$

Armed with Eq. (17) [or equivalently Eq. (18)], the solution in Eq. (11) is now fully explicit. This solution is exact in the

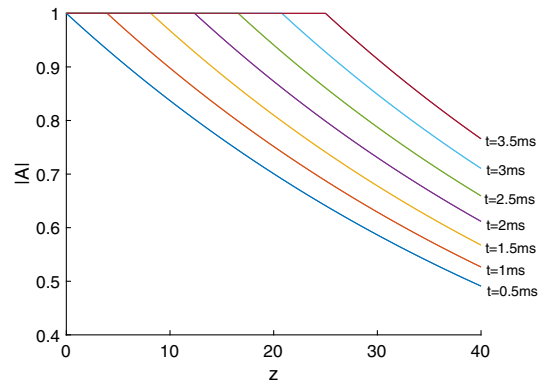


**Fig. 3.** Figure depicting the exact 1D solution in the first 40 m of a cloud with a 1 MW/cm<sup>2</sup> laser. The solution was sampled for this figure every 0.5 ms and only includes time when the pulse is on.

model, but as the model is approximate it should be considered as approximate for the physical penetration depth  $z_c(t)$  or tunneling time  $t_c(z)$ .

An example of the exact solution in space at equally spaced times is shown in Fig. 3. The change in decay rate from before  $z_c$  to after can be seen clearly. The figure depicts the exact one-dimensional solution in the first 40 m of a cloud with a 1 MW/cm<sup>2</sup> laser. The spatial step size used was  $\Delta z = 10^{-2}$  m. The pulse on time for this example is  $t_{on} = 4.1810 \times 10^{-4}$  s. The solution was sampled seven times at  $2.1 \times 10^{-7}$  s intervals.

#### 4. RADIALLY SYMMETRIC PARAXIAL EQUATION: NUMERICAL SIMULATIONS

In this section, we consider geometric effects on beam propagation by numerically simulating the radially symmetric paraxial equation, Eq. (1). The temperatures of a field of uniform diameter droplets and background gas (vapor only) are also tracked. The droplet field solves the piecewise defined Eq. (6), the background vapor solves the piecewise defined Eq. (9), and they are coupled via the boundary equation, Eq. (8).

Despite there only being one vapor temperature equation, there are two sources of vapor heating: the laser and the droplets. The laser heats the field of ambient vapor in the cloud, and that heat is able to diffuse on the same time scale, see Eq. (9). The heat flux from the droplet into the immediately surrounding vapor is tracked separately and is governed by the boundary equation, Eq. (8). The resultant vapor temperatures are then combined via the rule of mixtures,

$$T_v = T_{v,ambient} (1 - P_v) + T_{v,local} P_v, \quad (19)$$

where

$$\begin{aligned}
 P_v &= 10^{-6} \left( \frac{D_v}{D_0} \right)^3 \\
 &= 1.25 \times 10^{-4} \frac{D}{D_0},
 \end{aligned}$$

such that  $10^{-6}$  is the droplet concentration in the cloud used earlier in Eq. (3), and  $D_v = 5D$  is the diameter of the sphere of local vapor. The size of the local vapor was determined based

upon the domain over which the heat flux from the droplet is significant. Compared to Eq. (3), the reduced ratio of vapor volume to droplet volume is included here to account for the additional volume taken up by the vapor local to the droplet. The ratio is further simplified to demonstrate how the droplet concentration is related to the ratio of local vapor, which is heated by heat flux from the droplet, to ambient vapor, which is heated directly by the laser.

The numerical method used to solve the system of equations is a classic split-step scheme. It begins by solving the laser equation in space for a fixed time using the Crank–Nicholson scheme with zero boundary conditions. Then, the pulse on the temperature equation is solved in both the droplets and vapor with previously determined laser irradiance using Euler’s method. The droplet distribution is updated next, based on the temperature solution. Any droplets with a discrete internal temperature at or exceeding the critical temperature are replaced by vapor of the same temperature. The scheme is repeated for the duration of a pulse.

Between pulses, the dissipation of built up heat in the droplets and vapor is modeled by the heat equation. Within the droplets and in the vapor in the near vicinity of the droplets, the heat dissipation and transfer is modeled in one dimension and is solved using the Crank–Nicholson scheme. For the rest of the vapor, the heat equation is solved using the alternating direction implicit (ADI) method [64]. The large-scale vapor field temperature heated by the laser is tracked separately from the near-droplet vapor temperature. Specifically, the near-droplet vapor temperature is an average of the near-droplet vapor temperature over the locally solved domain and, once the droplet has exploded, includes the vapor that replaces the exploded droplets. The combined effect of these two vapor temperature fields on the laser is represented artificially through the rule of mixtures,

similar to effect of the droplets and vapor. The large-scale vapor field temperature and the averaged local vapor temperature are shown in Fig. 4.

Parameters, such as pulse length and irradiance, were chosen to satisfy the underlying assumptions of our model. As discussed earlier, irradiance between  $10^4$  W/cm<sup>2</sup> and  $10^8$  W/cm<sup>2</sup> is necessary to avoid plasma formation while allowing shattering to dominate droplet dynamics. Our model used an irradiance of  $10^6$  W/cm<sup>2</sup>. The cloud will be modeled as a cylinder with a radius of 3 m and length of 100 m. The laser model will operate with a pulse on time of  $t_{\text{on}} = 4.185 \times 10^{-6}$  s, a pulse off time of  $t_{\text{off}} = 8.069 \times 10^{-5}$  s, radial step size  $\Delta x = 5 \times 10^{-2}$ , azimuthal step size  $\Delta z = 10^{-2}$ , and initial Gaussian laser profile of

$$A(r, 0, 0) = e^{-r^2} \text{ MW/cm}^2.$$

Figure 5 shows the laser irradiance over two-dimensional, radially symmetric space for a sampling of times,  $t = 8.5 \times 10^{-5}$  s (after the first pulse and cooling period),  $t = 1.70 \times 10^{-4}$  s (after the second pulse and cooling period), and  $t = 1.71 \times 10^{-4}$  s (the time at which the laser has fully cleared a path through the cloud). Figure 6 shows the maximum temperature within each drop over two-dimensional, radially symmetric space for the same times as well as the cleared channel through the cloud (represented by the white space). The majority of the energy delivered by the laser goes to those droplets along the thin boundary between the cleared channel and the rest of the cloud. The maximum ambient vapor temperature and the maximum locally averaged vapor temperature are found to be  $0.45^\circ\text{C}$  and  $20.11^\circ\text{C}$  greater than the initial vapor temperature, respectively.

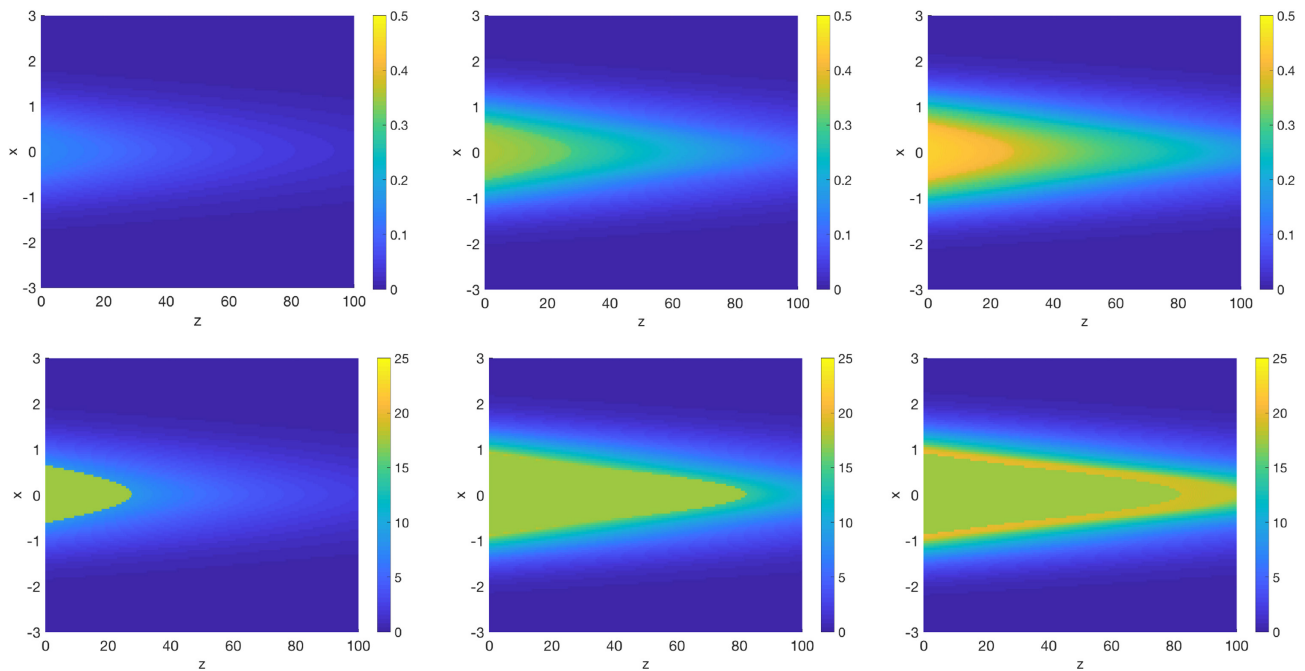


**Fig. 4.** Temperature fluctuations above  $23^\circ\text{C}$  of the ambient vapor, the vapor of the propagating medium heated by the laser (top row), and local vapor, the vapor immediately surrounding the drops heated through surface heat flux from the droplets (bottom row), over two-dimensional, radially symmetric space for time  $t = 8.5 \times 10^{-5}$  s,  $t = 1.70 \times 10^{-4}$  s, and  $t = 1.71 \times 10^{-4}$  s as a megawatt laser passes through a 100 m cloud.

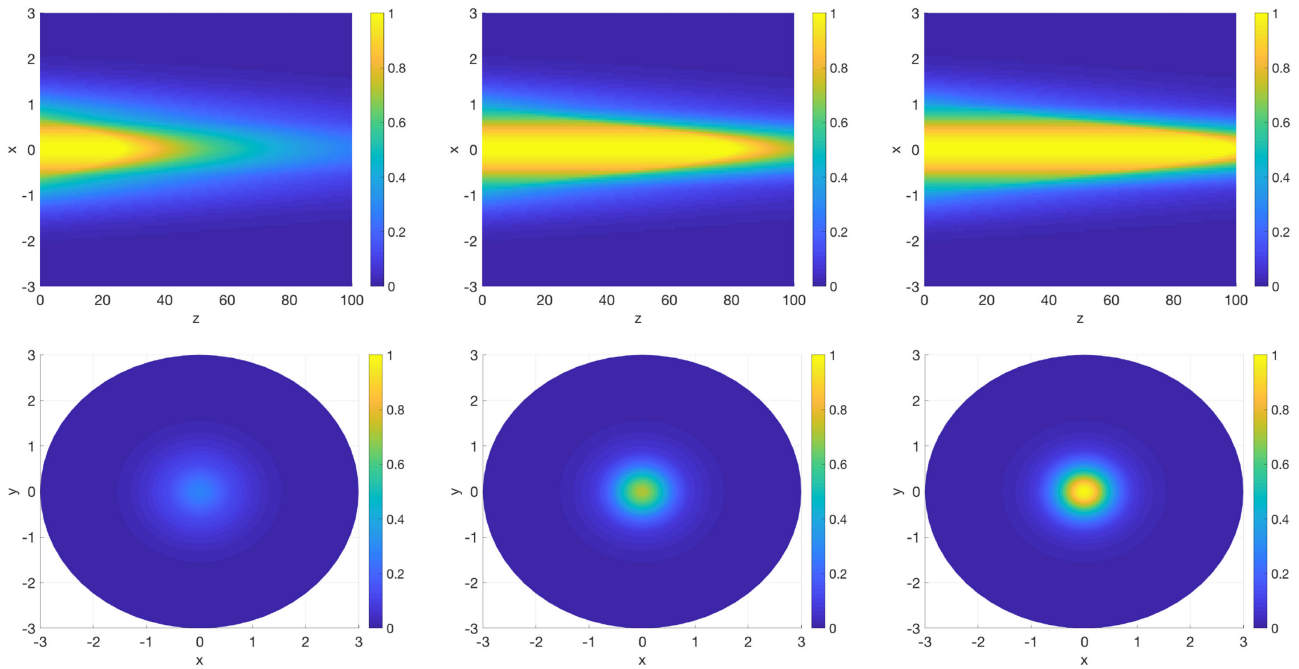


**Fig. 5.** Irradiance of the laser, sliced in the  $xz$  plane (top row) and at the back of the cloud  $z = 100$  m (bottom row) for times  $t = 8.5 \times 10^{-5}$  s,  $t = 1.70 \times 10^{-4}$  s, and  $t = 1.71 \times 10^{-4}$  s.

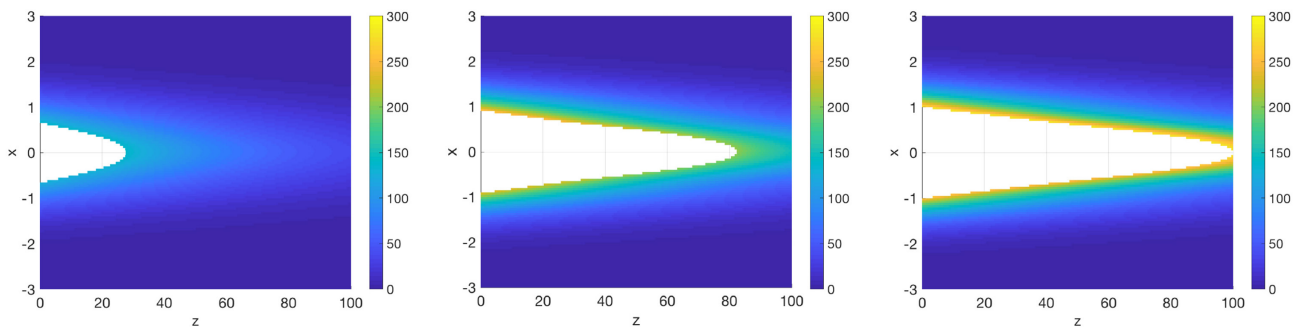


**Fig. 6.** Maximum temperature within each droplet over two-dimensional, radially symmetric space for time  $t = 8.5 \times 10^{-5}$  ms,  $t = 1.70 \times 10^{-4}$  ms, and  $t = 1.71 \times 10^{-4}$  ms. In the white central region, the droplets have exploded, and there is no droplet temperature to be represented.

### 5. DISCUSSION

The model presented in the previous section predicts dwell times and power input requirements for cloud clearing by high energy lasers. A one-dimensional model, which ignores beam shape, diffraction, and pulsing, and an axisymmetric, three-dimensional model were simulated. Both models showed that cloud clearing is possible in the same power regime. The assumptions used to derive this model are in many respects ideal, with some even hand-picked to allow for clearing to occur. In this section, we will discuss the limitations these assumptions place on the model, and the costs one would pay to relax them.

The presence of impurities in the droplet will deform the heating profile, potentially slowing down the shattering process. Impurities, however, will also provide a surface for vapor nucleation, causing droplets to explode at lower temperatures and allowing for quicker penetration time. Careful modeling of this effect requires knowledge of the impurities absorption

properties and simulation of the electromagnetic field within the impure drop.

The model maintains an implicit assumption that the laser acts on the entire cloud at once (the front of the laser entering the cloud is not tracked). This limits the maximum pulse frequency for which the model is valid. For example, a cloud depth of 100 m [25] requires that the pulse be no shorter than  $3 \times 10^{-7}$  s or 0.3  $\mu$ s (and preferably an order of magnitude longer). Ignoring this restriction would require tracking the front and back of the laser passing through the cloud. This could, in principle, be done numerically, but it destroys the structure used to derive the exact solution.

This model is limited to 10.6  $\mu$ m lasers. A change in wavelength will alter the heating profile of the drops. The heating profile is also specific to 10  $\mu$ m diameter drops; both smaller and larger drops have different heating profiles. The ratio between the wavelength and the droplet size presented in this model was chosen to produce the most distinct hot spot. Therefore any

deviation will produce less effective droplet shattering. For a given wavelength, smaller droplets have more uniform source functions and thus take longer to shatter. Droplets with a diameter larger than 10  $\mu\text{m}$  have a less centralized maximum and also require more time to shatter. As the hot spots become less distinct, more time will be required for the internal temperature of the droplet to reach the critical temperature. For longer exposure times, effects such as evaporation and droplet motion become more important, and would need to be incorporated.

The model takes the entire fluid system to be spatially static, no fluid motion is permitted. This can be thought of as a time-scale restriction, assuming that the laser heating happens on a faster time scale than any motion of the fluid, whether it be due to cross wind, vapor convection, or droplet motion. While the tracking of individual droplet motion is impractical, a model that incorporates droplet motion via tracking their distribution would be a natural extension of this work.

In order to quantify the assumption of a quiescent atmosphere, consider a wind speed of 30 mph and a cleared channel width of 1 m. The assumption of stationary droplets with respect to the laser effects only holds true if the laser can penetrate in less than 0.0357 s. That is the time it takes for a droplet to cross half the diameter of the cleared channel. Based on our simulation, the laser penetrated the cloud in 0.16 ms, an order of magnitude faster than necessary for the static droplet assumption. The persistence of this cleared channel is, of course, inversely proportional to wind speed.

The rule of mixtures used in vapor and droplet heating also directly influences the cloud clearing abilities of the laser based on the droplet density of the modeled cloud. A cloud with a higher density of droplets will increase the rule of mixtures fraction, affecting both the rate at which droplets explode and the rate at which the vapor heats.

The background gas was assumed to be pure water vapor, thereby overstating its effect on the laser. The effect of the water vapor on the laser was found to be minimal. A more accurate refractive index would correspond to a background vapor composed primarily of air and only about 1% water vapor. A more realistic background medium would then absorb less heat, allowing the laser to be more effective.

In this work, a monodisperse uniform field of droplets is used as a simple model for a cloud. Actual clouds are polydisperse, with non-uniform droplet locations. The 10  $\mu\text{m}$  diameter chosen here is the peak of the distribution of diameters observed in clouds [50] (as opposed to fog, haze, or rain, which all have other representative diameters). The drops whose sizes differ by an order of magnitude from 10  $\mu\text{m}$  have entirely different responses from those modeled here (important geometric effects within larger drops and dominant evaporation for smaller drops). A more realistic cloud model would require incorporation of these effects as well, but could in principle improve the accuracy of the model.

## 6. CONCLUSIONS AND FUTURE RESEARCH

The model presented above simulates the process of a high energy laser penetrating a cloud. This work considers the leading-order effects on the cloud clearing problem, creating an approximate model, for which exact solutions and numerical

simulations are presented. In the context of this model, it is shown that a channel can be cleared in a model cloud by a high energy 10.6  $\mu\text{m}$  laser.

A number of amendments to this model could be considered as avenues for future work. These can include non-axisymmetric beam geometries, the inclusion of a distribution of droplet sizes, and corresponding heating profiles. As mentioned before, these different heating profiles will be less effective, and evaporation may need to be incorporated. Ejected mass due to droplet shattering is not currently accounted for and should ultimately be tracked. Also, any resultant fluid flow from the explosions will appreciably affect the model but requires the simulation of the entire vapor velocity field.

**Funding.** Air Force Office of Scientific Research (APSHELs); Office of Naval Research (Radial Basis Functions for Numerical Simulation).

**Acknowledgment.** The authors thank Steven Fiorino, Jonah Reeger, and Joseph Coffaro for helpful discussions.

**Disclaimer.** This report was prepared as an account of work sponsored by an agency of the United States Government. Neither the United States Government nor any agency thereof, nor any of their employees, make any warranty, express or implied, or assumes any legal liability or responsibility for the accuracy, completeness, or usefulness of any information, apparatus, product, or process disclosed, or represents that its use would not infringe privately owned rights. Reference herein to any specific commercial product, process, or service by trade name, trademark, manufacturer, or otherwise does not necessarily constitute or imply its endorsement, recommendation, or favoring by the United States Government or any agency thereof. The views and opinions of the authors expressed herein do not necessarily state or reflect those of the United States Government or any agency thereof.

**Disclosures.** The authors declare no conflicts of interest.

## REFERENCES

1. L. C. Andrews and R. L. Phillips, *Laser Beam Propagation Through Random Media* (SPIE, 2005), Vol. 1.
2. K. N. Liou, S.-C. Ou, Y. Takano, and J. Cetola, "Remote sensing of three-dimensional cirrus clouds from satellites: application to continuous-wave laser atmospheric transmission and backscattering," *Appl. Opt.* **45**, 6849–6859 (2006).
3. R. J. Bartell, G. P. Perram, S. T. Fiorino, S. N. Long, M. J. Houle, C. A. Rice, Z. P. Manning, D. W. Bunch, M. J. Krizo, and L. E. Gravley, "Methodology for comparing worldwide performance of diverse weight-constrained high energy laser systems," *Proc. SPIE* **5792**, 1–13 (2005).
4. B. P. Abbott, R. Abbott, R. Adhikari, P. Ajith, B. Allen, G. Allen, R. S. Amin, S. B. Anderson, W. G. Anderson, M. A. Arain, M. Araya, H. Armandula, P. Armor, Y. Aso, S. Aston, P. Aufmuth, C. Aulbert, S. Babak, P. Baker, S. Ballmer, C. Barker, D. Barker, B. Barr, P. Barriga, L. Barsotti, M. A. Barton, I. Bartos, R. Bassiri, M. Bastarriga, B. Behnke, M. Benacquista, J. Betzwieser, P. T. Beyersdorf, I. A. Bilenko, G. Billingsley, R. Biswas, E. Black, J. K. Blackburn, L. Blackburn, D. Blair, B. Bland, T. P. Bodiya, L. Bogue, R. Bork, V. Boschi, S. Bose, P. R. Brady, V. B. Braginsky, J. E. Brau, D. O. Bridges, M. Brinkmann, A. F. Brooks, D. A. Brown, A. Brummit,

- G. Brunet, A. Bullington, A. Buonanno, O. Burmeister, R. L. Byer, L. Cadonati, J. B. Camp, J. Cannizzo, K. C. Cannon, J. Cao, L. Cardenas, S. Caride, G. Castaldi, S. Caudill, M. Cavaglià, C. Cepeda, T. Chalermongsak, E. Chalkley, P. Charton, S. Chatterji, S. Chelkowski, Y. Chen, N. Christensen, C. T. Y. Chung, D. Clark, J. Clark, J. H. Clayton, T. Cokelaer, C. N. Colacino, R. Conte, D. Cook, T. R. C. Corbitt, N. Cornish, D. Coward, D. C. Coyne, J. D. E. Creighton, T. D. Creighton, A. M. Cruise, R. M. Culter, A. Cumming, L. Cunningham, S. L. Danilishin, K. Danzmann, B. Daudert, G. Davies, E. J. Daw, D. DeBra, J. Degallaix, V. Dergachev, S. Desai, R. DeSalvo, S. Dhurandhar, M. Díaz, A. Dietz, F. Donovan, K. L. Dooley, E. E. Doomes, R. W. P. Drever, J. Dueck, I. Duke, J.-C. Dumas, J. G. Dwyer, C. Echols, M. Edgar, A. Effler, P. Ehrens, E. Espinoza, T. Etzel, M. Evans, T. Evans, S. Fairhurst, Y. Faltas, Y. Fan, D. Fazi, H. Fehrmenn, L. S. Finn, K. Flasch, S. Foley, C. Forrest, N. Fotopoulos, A. Franzen, M. Frede, M. Frei, Z. Frei, A. Freise, R. Frey, T. Fricke, P. Fritschel, V. V. Frolov, M. Fyffe, V. Galdi, J. A. Garofoli, I. Gholami, J. A. Giaime, S. Giampanis, K. D. Giardino, K. Goda, E. Goetz, L. M. Goggin, G. González, M. L. Gorodetsky, S. Goßler, R. Gouaty, A. Grant, S. Gras, C. Gray, M. Gray, R. J. S. Greenhalgh, A. M. Gretarsson, F. Grimaldi, R. Grosso, H. Grote, S. Grunewald, M. Guenther, E. K. Gustafson, R. Gustafson, B. Hage, J. M. Hallam, D. Hammer, G. D. Hammond, C. Hanna, J. Hanson, J. Harms, G. M. Harry, I. W. Harry, E. D. Harstad, K. Haughian, K. Hayama, J. Heefner, I. S. Heng, A. Heptonstall, M. Hewitson, S. Hild, E. Hirose, D. Hoak, K. A. Hodge, K. Holt, D. J. Hosken, J. Hough, D. Hoyland, B. Hughey, S. H. Huttner, D. R. Ingram, T. Isogai, M. Ito, A. Ivanov, B. Johnson, W. W. Johnson, D. I. Jones, G. Jones, R. Jones, L. Ju, P. Kalmus, V. Kalogera, S. Kandhasamy, J. Kanner, D. Kasprzyk, E. Katsavounidis, K. Kawabe, S. Kawamura, F. Kawazoe, W. Kells, D. G. Keppel, A. Khalaidovski, F. Y. Khalili, R. Khan, E. Khazanov, P. King, J. S. Kissel, S. Klimenko, K. Kokeyama, V. Kondrashov, R. Kopparapu, S. Koranda, D. Kozak, B. Krishnan, R. Kumar, P. Kwee, P. K. Lam, M. Landry, B. Lantz, A. Lazzarini, H. Lei, M. Lei, N. Leindecker, I. Leonor, C. Li, H. Lin, P. E. Lindquist, T. B. Littenberg, N. A. Lockerbie, D. Lodhia, M. Longo, M. Lormand, P. Lu, M. Lubinski, A. Lucianetti, H. Lück, B. Machenschalk, M. MacInnis, M. Mageswaran, K. Mailand, I. Mandel, V. Mandic, S. Márka, Z. Márka, A. Markosyan, J. Markowitz, E. Maros, I. W. Martin, R. M. Martin, J. N. Marx, K. Mason, F. Matichard, L. Matone, R. A. Matzner, N. Mavalvala, R. McCarthy, D. E. McClelland, S. C. McGuire, M. McHugh, G. McIntyre, D. J. A. McKechn, K. McKenzie, M. Mehmet, A. Melatos, A. C. Melissinos, D. F. Menéndez, G. Mendell, R. A. Mercer, S. Meshkov, C. Messenger, M. S. Meyer, J. Miller, J. Minelli, Y. Mino, V. P. Mitrofanov, G. Mitselmakher, R. Mittleman, O. Miyakawa, B. Moe, S. D. Mohanty, S. R. P. Mohapatra, G. Moreno, T. Morioka, K. Mors, K. Mossavi, C. MowLowry, G. Mueller, H. Müller-Ebhardt, D. Muhammad, S. Mukherjee, H. Mukhopadhyay, A. Mullavey, J. Munch, P. G. Murray, E. Myers, J. Myers, T. Nash, J. Nelson, G. Newton, A. Nishizawa, K. Numata, J. O'Dell, B. O'Reilly, R. O'Shaughnessy, E. Ochsner, G. H. Ogin, D. J. Ottaway, R. S. Ottens, H. Overmier, B. J. Owen, Y. Pan, C. Pankow, M. A. Papa, V. Parameshwaraiah, P. Patel, M. Pedraza, S. Penn, A. Perraca, V. Pierro, I. M. Pinto, M. Pitkin, H. J. Pletsch, M. V. Plissi, F. Postiglione, M. Principe, R. Prix, L. Prokhorov, O. Punken, V. Quetschke, F. J. Raab, D. S. Rabeling, H. Radkins, P. Raffai, Z. Raics, N. Rainer, M. Rakhmanov, V. Raymond, C. M. Reed, T. Reed, H. Rehbein, S. Reid, D. H. Reitze, R. Riesen, K. Riles, B. Rivera, P. Roberts, N. A. Robertson, C. Robinson, E. L. Robinson, S. Roddy, C. Röver, J. Rollins, J. D. Romano, J. H. Romie, S. Rowan, A. Rüdiger, P. Russell, K. Ryan, S. Sakata, L. S. de la Jordana, V. Sandberg, V. Sannibale, L. Santamaría, S. Saraf, P. Sarin, B. S. Sathyaprakash, S. Sato, M. Satterthwaite, P. R. Saulson, R. Savage, P. Savov, M. Scanlan, R. Schilling, R. Schnabel, R. Schofield, B. Schulz, B. F. Schutz, P. Schwinberg, J. Scott, S. M. Scott, A. C. Searle, B. Sears, F. Seifert, D. Sellers, A. S. Sengupta, A. Sergeev, B. Shapiro, P. Shawhan, D. H. Shoemaker, A. Sibley, X. Siemens, D. Sigg, S. Sinha, A. M. Sintes, B. J. J. Slagmolen, J. Slutsky, J. R. Smith, M. R. Smith, N. D. Smith, K. Somiya, B. Sorazu, A. Stein, L. C. Stein, S. Steplewski, A. Stochino, R. Stone, K. A. Strain, S. Strigin, A. Stroerer, A. L. Stuver, T. Z. Summerscales, K.-X. Sun, M. Sung, P. J. Sutton, G. P. Szokoly, D. Talukder, L. Tang, D. B. Tanner, S. P. Tarabrin, J. R. Taylor, R. Taylor, J. Thacker, K. A. Thorne, A. Thüring, K. V. Tokmakov, C. Torres, C. Torrie, G. Traylor, M. Trias, D. Ugolini, J. Ulmen, K. Urbanek, H. Vahlbruch, M. Vallisneri, C. Van Den Broeck, M. V. van der Sluys, A. A. van Veggel, S. Vass, R. Vaulin, A. Vecchio, J. Veitch, P. Veitch, C. Veltkamp, A. Villar, C. Vorvick, S. P. Vyachanin, S. J. Waldman, L. Wallace, R. L. Ward, A. Weidner, M. Weinert, A. J. Weinstein, R. Weiss, L. Wen, S. Wen, K. Wette, J. T. Whelan, S. E. Whitcomb, B. F. Whiting, C. Wilkinson, P. A. Willems, H. R. Williams, L. Williams, B. Willke, I. Wilmot, L. Winkelmann, W. Winkler, C. C. Wipf, A. G. Wiseman, G. Woan, R. Wooley, J. Worden, W. Wu, I. Yakushin, H. Yamamoto, Z. Yan, S. Yoshida, M. Zanolin, J. Zhang, L. Zhang, C. Zhao, N. Zotov, M. E. Zucker, H. zur Mühlen, and J. Zweigig, "LIGO: the laser interferometer gravitational-wave observatory," *Rep. Prog. Phys.* **72**, 076901 (2009).
5. R. L. Armstrong, S. A. W. Gerstl, and A. Zardecki, "Nonlinear pulse propagation in the presence of evaporating aerosols," *J. Opt. Soc. Am. B*, **2**, 1739–1746 (1985).
  6. K. D. Egorov, V. P. Kandidov, and S. S. Chesnokov, "Numerical analysis of the propagation of high-intensity laser radiation in the atmosphere," *Sov. Phys. J.* **26**, 161–173 (1983).
  7. A. V. Kuzikovskii, L. K. Chistyakova, and V. I. Kokhanov, "Pulsed clearing of a synthetic aqueous aerosol by CO<sub>2</sub> laser radiation," *Sov. J. Quantum Electron.* **11**, 1277–1281 (1981).
  8. V. E. Zuev and Y. D. Kopytin, "Nonlinear propagation of intense light in a gaseous medium with solid microfilling," *Sov. Phys. J.* **20**, 1458–1479 (1977).
  9. R. J. Lipinski and R. F. Walter, "Hole-boring through clouds for laser power beaming," *Proc. SPIE* **2376**, 1–10 (1995).
  10. D. R. Johnston and D. E. Burch, "Attenuation by artificial fogs in the visible, near infrared, and far infrared," *Appl. Opt.* **6**, 1497–1501 (1967).
  11. M. M. Colavita, M. R. Swain, R. L. Akeson, C. D. Koresko, and R. J. Hill, "Effects of atmospheric water vapor on infrared interferometry," *Publ. Astron. Soc. Pac.* **116**, 876–885 (2004).
  12. H. Matsumoto, "The refractivities of water vapour for CO<sub>2</sub> laser lines," *Opt. Commun.* **50**, 356–358 (1984).
  13. J. G. Xie, T. E. Ruekgauer, R. L. Armstrong, and R. G. Pinnick, "Evaporative instability in pulsed laser-heated droplets," *Phys. Rev. Lett.* **66**, 2988–2991 (1991).
  14. A. P. Waggoner, L. F. Radke, V. Buonadonna, and D. R. Dowling, "Cloud clearing with a CO<sub>2</sub>-laser in a cirrus cloud simulation facility," *Appl. Opt.* **31**, 5871–5877 (1992).
  15. G. P. Quigley, R. B. Webster, E. J. Caramana, R. L. Morse, and G. W. York, "Cloud hole boring with long pulse CO<sub>2</sub> lasers: theory and experiment," *Appl. Opt.* **30**, 3041–3046 (1991).
  16. E. J. Caramana, J. L. Kindel, R. L. Morse, G. P. Quigley, R. B. Webster, and G. W. York, "Droplet shattering, vaporization and recondensation in cloud clearing with long pulse infrared chemical lasers," Technical Report NTIS, PC A02/MF A01—OSTI (Los Alamos National Laboratory, 1990).
  17. M. Autric, P. Vigliano, D. Dufresne, J. P. Caressa, and P. Bournot, "Pulsed CO<sub>2</sub> laser-induced effects on water droplets," *AIAA J.* **26**, 65–71 (1988).
  18. M. C. Fowler, "Effect of a CO<sub>2</sub> laser pulse on transmission through fog at visible and IR wavelengths," *Appl. Opt.* **22**, 2960–2964 (1983).
  19. B.-S. Park and R. L. Armstrong, "Laser droplet heating: fast and slow heating regimes," *Appl. Opt.* **28**, 3671–3680 (1989).
  20. R. L. Armstrong and A. Zardecki, "Diffusive and convective vaporization of irradiated droplets," *J. Appl. Phys.* **62**, 4571–4578 (1987).
  21. S. M. Chitanvis and S. A. W. Gerstl, "Aerosol clearing model for a high-energy laser beam propagating through vaporizing media," *J. Appl. Phys.* **62**, 3091–3096 (1987).
  22. C. T. Lee, T. G. Miller, and R. W. Jones, "Fog dispersal by CO<sub>2</sub> laser pulses: an exact solution including prevaporization heating," *Appl. Opt.* **21**, 428–432 (1982).
  23. A. H. Aitken, J. N. Hayes, and P. B. Ulrich, "Propagation of high-energy 10.6-micron laser beams through the atmosphere," Tech. Rep. 7293 (Naval Research Laboratory, 1971).
  24. S. Pineda, "Numerical simulation of laser-induced drop evaporation," Tech. Rep. (Naval Academy Annapolis, 2019).
  25. R. R. Rogers and M. K. Yau, *A Short Course in Cloud Physics*, 3rd ed. (Butterworth-Heinemann, 1996).

26. J. D. Pendleton, "Water droplets irradiated by a pulsed CO<sub>2</sub> laser: comparison of computed temperature contours with explosive vaporization patterns," *Appl. Opt.* **24**, 1631–1637 (1985).
27. A. P. Prishivalko and S. T. Leiko, "Radiative heating and evaporation of droplets," *J. Appl. Spectrosc.* **33**, 1137–1143 (1980).
28. A. P. Prishivalko, "Heating and destruction of water drops on exposure to radiation with inhomogeneous internal heat evolution," *Sov. Phys. J.* **26**, 142–148 (1983).
29. R. Cole, "Boiling nucleation," *Adv. Heat Transfer* **10**, 85–166 (1974).
30. V. P. Skripov, *Metastable Liquids* (Wiley, 1974).
31. R. G. Pinnick, A. Biswas, R. L. Armstrong, S. G. Jennings, J. D. Pendleton, and G. Fernández, "Micron-sized droplets irradiated with a pulsed CO<sub>2</sub> laser: measurement of explosion and breakdown thresholds," *Appl. Opt.* **29**, 918–925 (1990).
32. B.-S. Park, A. Biswas, R. L. Armstrong, and R. G. Pinnick, "Delay of explosive vaporization in pulsed laser-heated droplets," *Opt. Lett.* **15**, 206–208 (1990).
33. K. Hiraoka, K. Murata, K. Aizawa, F. Matsushita, H. Fukasawa, and T. Sato, "Explosive vaporization of a liquid water beam by irradiation with a 10.6- $\mu\text{m}$  infrared laser," *Rapid Commun. Mass Spectrom.* **11**, 474–478 (1997).
34. C. C. Tseng and R. Viskanta, "Enhancement of water droplet evaporation by radiation absorption," *Fire Saf. J.* **41**, 236–247 (2006).
35. G. Miliauskas, "Regularities of unsteady radiative–conductive heat transfer in evaporating semitransparent liquid droplets," *Int. J. Heat Mass Transfer* **44**, 785–798 (2001).
36. G. Miliauskas and V. Šabanas, "Interaction of transfer processes during unsteady evaporation of water droplets," *Int. J. Heat Mass Transfer* **49**, 1790–1803 (2006).
37. G. Miliauskas and V. Šabanas, "Interacting heat transfer processes in water droplets," *Mechanics* **52**, 1–17 (2005).
38. A. Saha, S. Basu, and R. Kumar, "Scaling analysis: equivalence of convective and radiative heating of levitated droplet," *Appl. Phys. Lett.* **100**, 204104 (2012).
39. D. G. Fouche, C. Higgs, and C. F. Pearson, "Scaled atmospheric blooming experiments (SABLE)," *Linc. Lab. J.* **5**, 273–293 (1992).
40. D. C. Smith, "High-power laser propagation: thermal blooming," *Proc. IEEE* **65**, 1679–1714 (1977).
41. J. A. Fleck, J. R. Morris, and M. D. Feit, "Time-dependent propagation of high energy laser beams through the atmosphere," *Appl. Phys. A* **10**, 126–160 (1976).
42. F. G. Gebhardt, "Twenty-five years of thermal blooming: an overview," *Proc. SPIE* **1221**, 2–25 (1990).
43. V. A. Banakh and A. V. Falits, "Numerical simulation of propagation of laser beams formed by multielement apertures in a turbulent atmosphere under thermal blooming," *Atmos. Ocean. Opt.* **26**, 455–465 (2013).
44. V. A. Banakh and A. V. Falits, "Efficiency of combined beam focusing under thermal blooming," *Atmos. Ocean. Opt.* **27**, 211–217 (2014).
45. P. Sprangle, J. R. Peñano, A. Ting, and B. Hafizi, "Propagation of high-energy lasers in a maritime atmosphere," (Naval Research Labs, 2004).
46. J. R. Penano, P. Sprangle, and B. Hafizi, "Propagation of high energy laser beams through atmospheric stagnation zones," *Tech. Rep.* (Naval Research Lab, Beam Physics Branch, 2006).
47. W. Nelson, P. Sprangle, and C. C. Davis, "Atmospheric propagation and combining of high-power lasers," *Appl. Opt.* **55**, 1757–1764 (2016).
48. B. F. Akers and J. A. Reeger, "Numerical simulation of thermal blooming with laser-induced convection," *J. Electromagn. Waves Appl.* **33**, 1–11 (2018).
49. A. Zemlyanov, Y. E. Geints, A. Kabanov, and R. Armstrong, "Investigation of laser-induced destruction of droplets by acoustic methods," *Appl. Opt.* **35**, 6062–6068 (1996).
50. G. W. Sutton, "Fog hole boring with pulsed high-energy lasers: an exact solution including scattering and absorption," *Appl. Opt.* **17**, 3424–3430 (1978).
51. M. J. Ablowitz, *Nonlinear Dispersive Waves: Asymptotic Analysis and Solitons* (Cambridge University, 2011), Vol. **47**.
52. C. Sulem and P.-L. Sulem, *The Nonlinear Schrödinger Equation: Self-Focusing And Wave Collapse* (Springer, 2007), Vol. **139**.
53. A. V. Kuzikovskii, "Dynamics of a spherical particle in an intense optical field," *Russ. Phys. J.* **13**, 615–619 (1970).
54. P. Sprangle, E. Esarey, and A. Ting, "Nonlinear theory of intense laser-plasma interactions," *Phys. Rev. Lett.* **64**, 2011–2014 (1990).
55. A. Biswas, H. Latifi, P. Shah, L. J. Radziemski, and R. L. Armstrong, "Time-resolved spectroscopy of plasmas initiated on single, levitated aerosol droplets," *Opt. Lett.* **12**, 313–315 (1987).
56. J. H. Eickmans, W.-F. Hsieh, and R. K. Chang, "Laser-induced explosion of H<sub>2</sub>O droplets: spatially resolved spectra," *Opt. Lett.* **12**, 22–24 (1987).
57. M. Z. Martin, M.-D. Cheng, and R. C. Martin, "Aerosol measurement by laser-induced plasma technique: a review," *Aerosol Sci. Technol.* **31**, 409–421 (1999).
58. P. Polynkin, C. Ament, and J. V. Moloney, "Self-focusing of ultraintense femtosecond optical vortices in air," *Phys. Rev. Lett.* **111**, 023901 (2013).
59. G. Schimmel, T. Produit, D. Mongin, J. Kasparian, and J.-P. Wolf, "Free space laser telecommunication through fog," *Optica* **5**, 1338–1341 (2018).
60. P. E. Ciddor, "Refractive index of air: new equations for the visible and near infrared," *Appl. Opt.* **35**, 1566–1573 (1996).
61. A. Zemlyanov, V. Zuev, Y. Geints, and V. Pogodaev, "Propagation of intensive laser radiation in atmospheric aerosol," *Proc. SPIE* **2222**, 328–338 (1994).
62. E. J. Caramana, R. B. Webster, G. P. Quigley, and R. L. Morse, "Theoretical and experimental studies of CO<sub>2</sub> laser evaporation of clouds," *J. Appl. Phys.* **70**, 4601–4616 (1991).
63. S. T. Fiorino, R. J. Bartell, M. J. Krizo, G. L. Caylor, K. P. Moore, T. R. Harris, and S. J. Cusumano, "A first principles atmospheric propagation and characterization tool: the laser environmental effects definition and reference (LEEDR)," *Proc. SPIE* **6878**, 68780B (2008).
64. D. Peaceman and J. Rachford, "The numerical solution of parabolic and elliptic differential equations," *J. Soc. for Ind. Appl. Math.* **3**, 28–41 (1955).
65. R. J. Hill and R. S. Lawrence, "Refractive index of water vapor in infrared windows," *Infrared Phys.* **26**, 371–376 (1986).
66. M. E. Thomas, "Infrared- and millimeter-wavelength continuum absorption in the atmospheric windows: measurements and models," *Infrared Phys.* **30**, 161–174 (1990).